



## Low-Temperature, Low-Pressure Chemical Vapor Deposition and Solid Phase Crystallization of Silicon–Germanium Films

Munehiro Tada,<sup>a,b,z</sup> Jin-Hong Park,<sup>a</sup> Jinendra Raja Jain,<sup>a</sup> and Krishna C. Saraswat<sup>a</sup>

<sup>a</sup>Department of Electrical Engineering, Stanford University, Stanford, California 94305, USA

<sup>b</sup>NEC Corporation, Device Platforms Research Laboratories, Kanagawa, Japan

Low-pressure chemical vapor deposition of silicon–germanium ( $\text{Si}_{1-x}\text{Ge}_x$ ) and its SPC below  $400^\circ\text{C}$  are investigated. The effects of precursor ratio [ $\text{SiH}_4/\text{SiH}_2\text{Cl}_2$  (DCS): $\text{GeH}_4$ ], pressure, and temperature are examined with the goals of film composition tunability and high deposition rates.  $\text{SiH}_4$  is found to be a better source gas than DCS because the decomposition rate of  $\text{SiH}_4$  is faster than that of DCS during the deposition process. In the  $\text{SiH}_4:\text{GeH}_4$  system, the binary deposition mechanism is well explained by the “enhancement” model. The deposition temperature and chamber pressure affect the conversion factor, enabling independent tuning of the film composition and deposition rate. Amorphous  $\text{Si}_{0.7}\text{Ge}_{0.3}$  and  $\text{Si}_{0.5}\text{Ge}_{0.5}$  films are obtained at  $350$  and  $400^\circ\text{C}$  by adjusting the deposition conditions while keeping the deposition rates high. Compositional effects of the SiGe films on the SPC are also investigated.

© 2008 The Electrochemical Society. [DOI: 10.1149/1.3008009] All rights reserved.

Manuscript submitted August 21, 2008; revised manuscript received October 6, 2008. Published November 7, 2008.

In the past few decades, much attention has been devoted to silicon–germanium ( $\text{Si}_{1-x}\text{Ge}_x$ ) film growth because of applications in complementary metal oxide semiconductors (CMOSs),<sup>1</sup> high-frequency heterojunction bipolar transistors,<sup>2</sup> and high-efficiency solar cell technologies.<sup>3</sup> The  $\text{Si}_{1-x}\text{Ge}_x$  system has two advantages: a variable energy bandgap allowing bandgap engineering and high compatibility with Si-based processing. Especially important for the CMOS applications,  $\text{Si}_{1-x}\text{Ge}_x$  can be used as a low-resistivity gate electrode,<sup>4</sup> a higher mobility channel,<sup>5</sup> and a local strain enhancement layer through source and drain regions.<sup>6</sup> The other advantage of  $\text{Si}_{1-x}\text{Ge}_x$  is that it has a higher growth rate than Si at lower temperatures, which is useful for the low thermal budget processing required for thin-film transistors,<sup>7</sup> microelectromechanical system,<sup>8</sup> and monolithic three-dimensional ICs (3D-ICs).<sup>9,10</sup>

The monolithic 3D-IC technology reduces the length of interconnects, solving speed and power consumption problems by reducing wire capacitance. In addition, this technology provides increased logic density after the end of CMOS scaling and does not have a serious 3D wafer-to-wafer alignment problem. Although this is promising for future technology, 3D-IC fabrication is still challenging. Devices have to be fabricated above copper interconnects with fragile, porous, low dielectric constant materials<sup>11,12</sup> and devices for achieving 3D-ICs. A low-temperature process (at sub- $400^\circ\text{C}$ ), is thus required to preserve the underlying interconnects and devices.

Deposition of  $\text{Si}_{1-x}\text{Ge}_x$  films in low-pressure chemical vapor deposition (LPCVD) systems can be simply achieved by combining Si gaseous precursors [ $\text{SiH}_4$ ,  $\text{Si}_2\text{H}_6$ , and  $\text{SiCl}_2\text{H}_2$  (DCS)] and germane ( $\text{GeH}_4$ ).<sup>13</sup> Adding  $\text{GeH}_4$  gas enables reduction of the deposition temperature of  $\text{Si}_{1-x}\text{Ge}_x$  film because  $\text{GeH}_4$  has a higher reactivity than the Si source gases. Despite the lower deposition temperature, the  $\text{Si}_{1-x}\text{Ge}_x$  system has a considerably complicated mechanism. Therefore, several researchers have investigated the mechanisms and kinetics of the  $\text{Si}_{1-x}\text{Ge}_x$  growth.<sup>14–16</sup> Most of the  $\text{Si}_{1-x}\text{Ge}_x$  growth experiments in these papers have been conducted at temperatures between  $450$  and  $600^\circ\text{C}$ , which is relatively low compared to that used in Si depositions. However, the temperature range is still high for monolithic 3D-IC applications. Another potential difficulty in the low-temperature deposition of  $\text{Si}_{1-x}\text{Ge}_x$  films is tunability of film composition while keeping high deposition rates ( $>1$  nm/min) because the Si component exponentially decreases with the temperature. Details of the  $\text{Si}_{1-x}\text{Ge}_x$  deposition below  $400^\circ\text{C}$  have not been characterized yet.

This paper focuses on the deposition of  $\text{Si}_{1-x}\text{Ge}_x$  below  $400^\circ\text{C}$  for low-temperature applications. Mechanisms and kinetics of the  $\text{Si}_{1-x}\text{Ge}_x$  deposition are examined by adjusting the source gas ratio, chamber pressure, and substrate temperature. Compositional effects of the  $\text{Si}_{1-x}\text{Ge}_x$  film on its solid phase crystallization (SPC) are also investigated.

### Experimental

The starting substrates were  $100$  mm Si wafers (n-type,  $5\text{--}10$   $\Omega$  cm) with  $200$  nm silicon dioxide ( $\text{SiO}_2$ ) grown by wet thermal oxidation. The wafers were cleaned in  $4:1$   $\text{H}_2\text{SO}_4:\text{H}_2\text{O}_2$  at  $90^\circ\text{C}$  for  $10$  min and  $5:1:1$   $\text{H}_2\text{O}:\text{HCl}:\text{H}_2\text{O}_2$  at  $70^\circ\text{C}$  for  $10$  min, followed by a deionized water rinse and  $\text{N}_2$  drying. The  $\text{Si}_{1-x}\text{Ge}_x$  films were deposited in an LPCVD epi chamber (Applied Materials Epi Centura) using pure  $\text{SiH}_4$ ,  $\text{SiH}_2\text{Cl}_2$  (DCS), and  $\text{GeH}_4$  gases. Hydrogen gas of  $6$  slpm was used as a carrier gas. For comparison, depositions of both  $\alpha$ -Ge and  $\alpha$ -Si films were performed in a hot-wall tubular LPCVD furnace without the hydrogen carrier gas. Depositions were done at constant temperatures between  $300$  and  $550^\circ\text{C}$ . A few monolayers of Si were predeposited on  $\text{SiO}_2$  at  $500^\circ\text{C}$  for  $6$  min (in furnace), or  $550^\circ\text{C}$  for  $1$  min (in epi chamber) to provide nucleation sites when  $\text{GeH}_4$  was used during the film deposition.<sup>17</sup> To evaluate the SPC of the films, four kinds of amorphous films were prepared: amorphous ( $\alpha$ )-Si deposited at  $550^\circ\text{C}$ ,  $\alpha$ - $\text{Si}_{0.5}\text{Ge}_{0.5}$  at  $400^\circ\text{C}$ ,  $\alpha$ - $\text{Si}_{0.7}\text{Ge}_{0.3}$  at  $350^\circ\text{C}$ , and  $\alpha$ -Ge at  $300^\circ\text{C}$ . After the depositions, samples were annealed for  $1$  h in  $\text{N}_2$  ambient at several temperatures to evaluate the SPC.

X-ray photoelectron spectroscopy was used to measure the Ge fraction of the  $\text{Si}_{1-x}\text{Ge}_x$  films. The thickness of the deposited  $\text{Si}_{1-x}\text{Ge}_x$  films on  $\text{SiO}_2$  was determined by scanning electron microscopy. The composition and growth rate of the films were checked three times and the repeatability was confirmed. The crystal phases of the  $\text{Si}_{1-x}\text{Ge}_x$  films were examined by X-ray diffraction (XRD) (Cu K $\alpha$ ,  $\lambda = 1.5408$  Å).

### Results and Discussion

*Deposition of  $\text{Si}_{1-x}\text{Ge}_x$  film.*—Figure 1 presents the deposition rates of Si and Ge films using the respective  $\text{SiH}_4$  and  $\text{GeH}_4$  source gases as a function of the reciprocal of the deposition temperature. The deposition rates exponentially vary with the temperature, and both Si and Ge films show almost the same activation energy (around  $\sim 1.2$  eV), which is consistent with previous reports.<sup>18</sup> The deposition rate of Si is more than  $100\times$  smaller than that of Ge at the same temperature. This originates from a lower reactivity of  $\text{SiH}_4$  compared with  $\text{GeH}_4$ . In the  $\text{Si}_{1-x}\text{Ge}_x$  film deposition process,

<sup>z</sup> E-mail: m-tada@bl.jp.nec.com

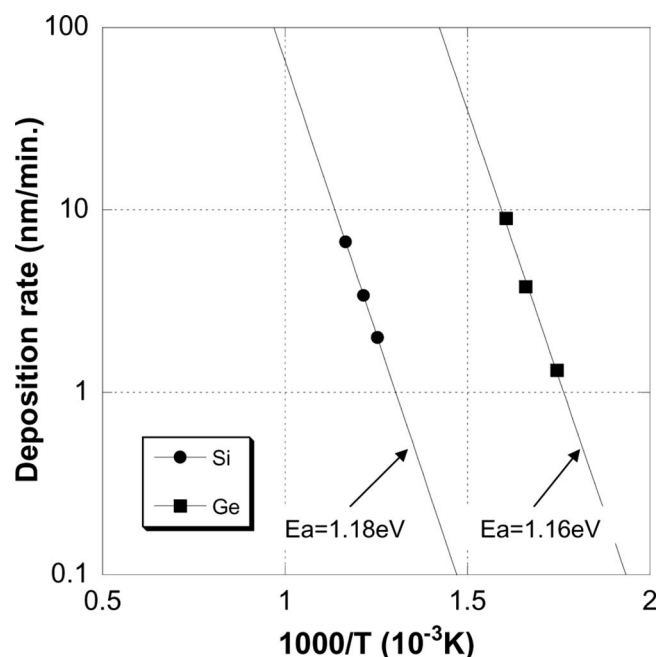


**Figure 1.** Deposition rates of Si and Ge using respective  $\text{SiH}_4$  and  $\text{GeH}_4$  source gases as a function of a reciprocal of the deposition temperature.

the “enhancement” model is often used to explain the relationship between the source gas ratio and the film composition.<sup>19</sup> The Ge fraction of the  $\text{Si}_{1-x}\text{Ge}_x$  film is enhanced by a constant factor,  $J$ . This behavior can be described by an equation of the following formula

$$\frac{x}{1-x} = J \times \frac{P_{\text{GeH}_4}}{P_{\text{SiH}_4}} \quad [1]$$

$J$  is the enhancement factor and  $x$  is the Ge atomic fraction of the film.  $P_{\text{GeH}_4}$  and  $P_{\text{SiH}_4}$  are the respective partial pressures of the  $\text{SiH}_4$  and  $\text{GeH}_4$  in the deposition system. Equation 1 can be written in a fractional form

$$x = \frac{J \times f}{(1-f) + J \times f} \quad [2]$$

where  $f$  is defined as the  $\text{GeH}_4$  fraction of the source gases

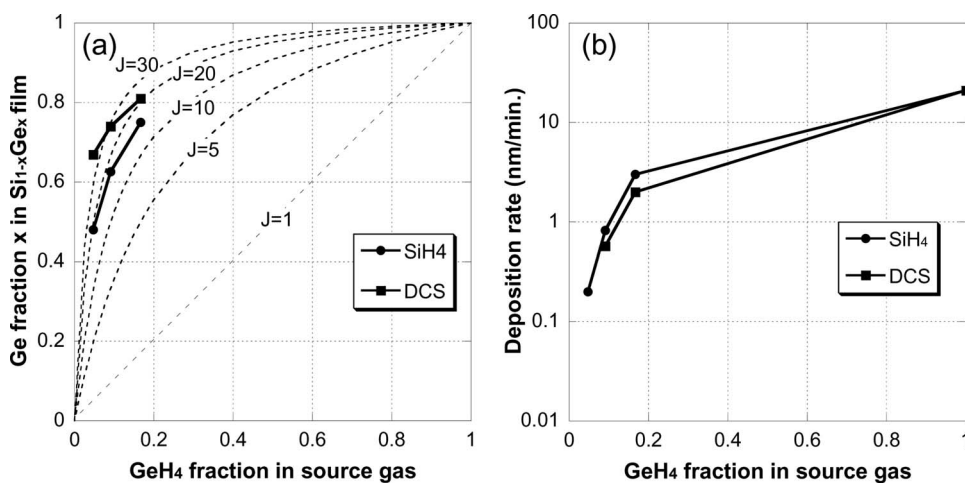
$$f = \frac{P_{\text{GeH}_4}}{P_{\text{SiH}_4} + P_{\text{GeH}_4}} \quad [3]$$

In this simple assumption, the  $J$  factor does not depend on the ratio of the source gases. Usually, the  $J$  factor in the  $\text{SiH}_4/\text{GeH}_4$  system is larger than 1, indicating that the Ge fraction of the film is higher than the  $\text{GeH}_4$  fraction in the source gas mixture.

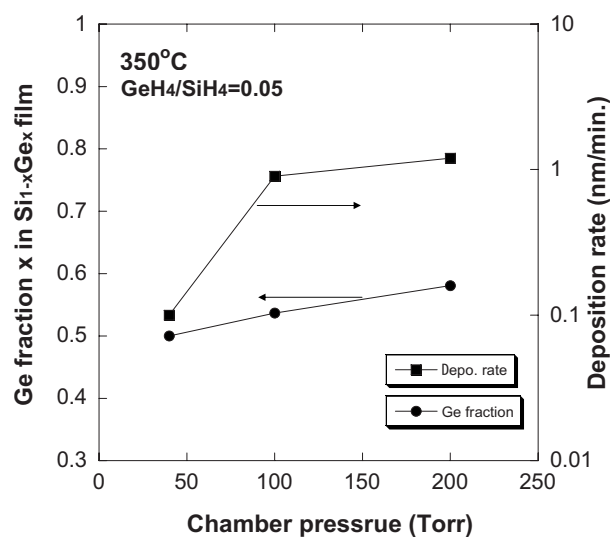
Figure 2 shows the Ge fraction and the deposition rates of the  $\text{Si}_{1-x}\text{Ge}_x$  films as a function of the  $\text{GeH}_4$  fraction in the source gas mixture, where the two kinds of the Si source gases ( $\text{SiH}_4$  and DCS) are evaluated. The deposition temperature and chamber pressure are kept at  $350^\circ\text{C}$  and 40 Torr, respectively. The dotted lines are calculated values with  $J$  factors of 1, 5, 10, 20, and 30. In the  $\text{SiH}_4$  system, the relation is well explained by the enhancement model, revealing that the  $J$  factor is estimated to be  $\sim 18$  and suggesting that it is difficult to increase the Si fraction of the film at  $350^\circ\text{C}$ . In the case of the DCS system, the relation shows a higher  $J$  factor than that in the  $\text{SiH}_4$  system and is not well-fitted to the enhancement model, having a large  $J$  factor range of 20–33.  $\text{SiH}_4$  provides a higher deposition rate than DCS. It is assumed that the decomposition rate of DCS is slower than that of  $\text{SiH}_4$  at the low temperature below  $400^\circ\text{C}$ . Therefore, the deposition rate and Si fraction of the film are reduced in the DCS system. The chlorine behavior complicates the deposition mechanism, causing imperfect fitting to the enhancement model. The film’s Ge fraction is manipulated in the range from  $x = 0.5$  to 1.0, while the deposition rate is very low (below 1 nm/min) at the lower  $\text{GeH}_4$  gas fraction of 0.05. Thus, deposition at low temperature ( $350^\circ\text{C}$ ) makes it more difficult to increase the Si fraction in the  $\text{Si}_{1-x}\text{Ge}_x$  film while keeping a high deposition rate. For the purpose of tuning the composition of the  $\text{Si}_{1-x}\text{Ge}_x$  film while keeping the high deposition rate, we chose  $\text{SiH}_4$  for the Si source gas in the following experiments, in which the  $\text{GeH}_4/\text{SiH}_4$  ratio is kept at 0.05. The effects of the chamber pressure and substrate temperature are examined.

Figure 3 shows the Ge fraction and the deposition rate of the films as a function of the chamber pressure. The substrate temperature is kept at  $350^\circ\text{C}$ . The Ge fraction is increased with the chamber pressure. The deposition rate increases with the chamber pressure. Thus, the higher pressure increases both the  $J$  factor and the deposition rate. We speculate that the higher pressure not only enhances the sticking coefficients of the source gases to the surface, but also suppresses the desorption from the surface, resulting in an increase of the deposition rate. The higher chamber pressure also increases the Ge fraction of the film, increasing the  $J$  factor, which may originate from a change in the balance between adsorption and desorption in the system.

Figure 4 shows the film Ge fraction as a function of the substrate



**Figure 2.** (a) Relationship between  $\text{GeH}_4$  in source gas and Ge fraction in film by using the different Si source gases. (b) Deposition rates of the films as a function of the  $\text{GeH}_4$  in source gases.



**Figure 3.** Ge fraction and deposition rate of the films as a function of the chamber pressure. The substrate temperature is kept at 350°C.

temperature. The temperature is kept at 350, 370, or 400°C, and the chamber pressure is maintained at 200 Torr. The Ge fraction is decreased as the temperature increases. This indicates that the  $J$  factor depends on the temperature, with the higher temperatures reducing the  $J$  factor. Figure 4b shows the deposition rate of the films as a function of the temperature. The deposition rate is increased with the temperature. The higher temperature enhances the decomposition and reaction of the source gases, resulting in the higher deposition rate. It is assumed that the desorption of Ge is enhanced more than that of Si at higher temperatures because the bond energy of Ge is lower than that of Si. Table I presents the bond strength of diatomic molecules.<sup>20</sup> The higher temperature enhances not only the adsorption of source gases to the surface, but also the desorption from the surface. The higher binding energy of Si contributes to keep the Si ratio in the film high. Thus, the high temperature facilitates low  $J$  factors while keeping the higher deposition rates.

Based on both the enhancement model and the dependencies on pressure and temperature, a deposition mechanism is described. Fig-

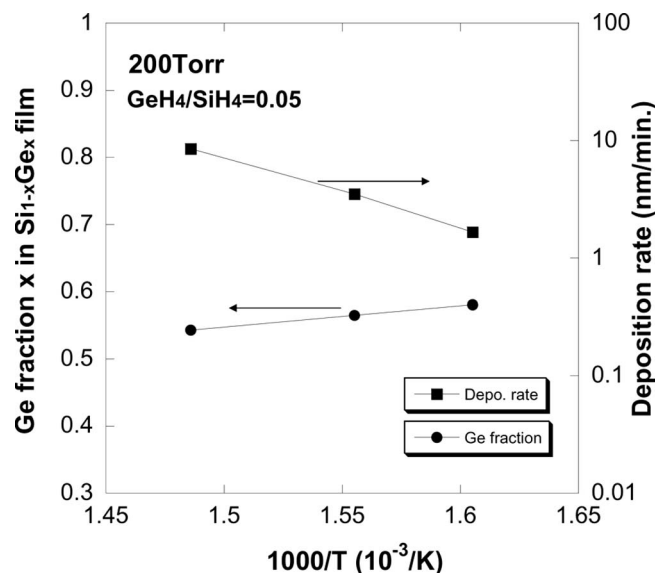


**Figure 4.** Ge fraction and deposition rate of the films as a function of the deposition temperature. The chamber pressure is maintained at 200 Torr.

**Table I.** Bond strength of diatomic molecules.

Diatomic molecule	Bond energy (eV)
Ge-Ge	2.7
Ge-Si	3.1
Si-Si	3.4

ure 5a shows a schematic model describing the sequence in the deposition of the  $\text{Si}_{1-x}\text{Ge}_x$  film. First, the source gases are thermally initiated as precursors and transported to the wafer surface, (i). A smaller binding energy of Ge-H (289 kJ/mol) than Si-H (323 kJ/mol) enhances the Ge precursor formation more than the Si precursor. Second, the initiated precursors are adsorbed on the surface, (ii) and (iii). Once on the surface, they diffuse until they eventually find a stable site, (iv) or are desorbed, (v). The hydrogen must be desorbed to complete the deposition step and make new nucleation sites, (vi).<sup>21</sup> Here, the deposition of atoms is defined as a total of the adsorption (iii) and desorption [(v) + (vi)]. A schematic image of the detail of the bindings is shown in Fig. 5b. Case (A) occurs with the higher probability in the system due to the highest reactivity of  $\text{GeH}_x$  to Ge. The probability of case (D) may be the smallest because the deposition of Si itself ( $\text{SiH}_x$  to Si) is very poor at 350°C (see Fig. 1). Therefore, the Si fraction of the film mainly depends on case (C). When the deposition temperature is increased, adsorptions in all cases are increased. In contrast, the desorptions depend on the bindings, where case (A) is easy to be decomposed and desorbed because the lower Ge-Ge bond energy promotes the desorption of Ge from the surface. In other words, Si-H is strongly adsorbed to Ge or to Si at the surface due to their high bond energy. Therefore, the high bond energy of Si contributes to the high Si fraction in the film at higher temperatures.

Figure 6 summarizes the relationship between the deposition rate and Ge fraction of the  $\text{Si}_{1-x}\text{Ge}_x$  films. With the deposition temperature and chamber pressure fixed at 350°C and 40 Torr, respectively, the deposition rate and Ge fraction of the film are decreased with the  $\text{GeH}_4$  ratio. The relation between the film composition and the gas ratio is well explained by the enhancement model based on the formula Eq. 1. When the chamber pressure is increased from 40 to 200 Torr, the deposition rate is increased while keeping almost the same Ge fraction of the film. Further increment of the deposition rate is achieved by increasing the temperature from 350 to 400°C. The Si fraction is also increased with the temperature. The precise adjustments of the source gas ratio, chamber pres-

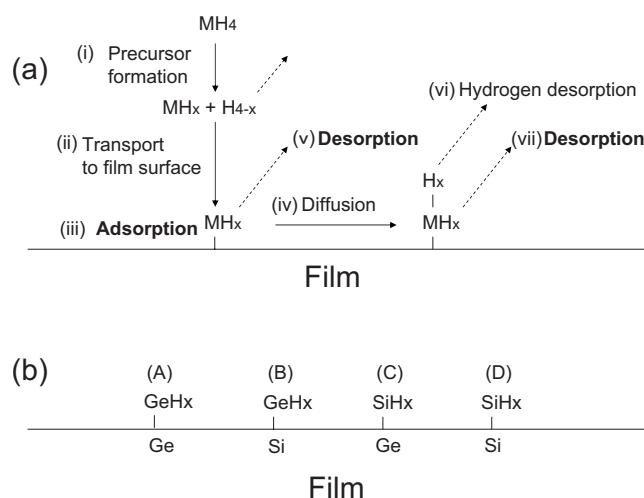


**Figure 5.** (a) Schematic model describing important steps in deposition of Si or Ge. (b) Conceptual diagram, showing the four possible scenarios where a single precursor molecule lands on the single surface atoms.

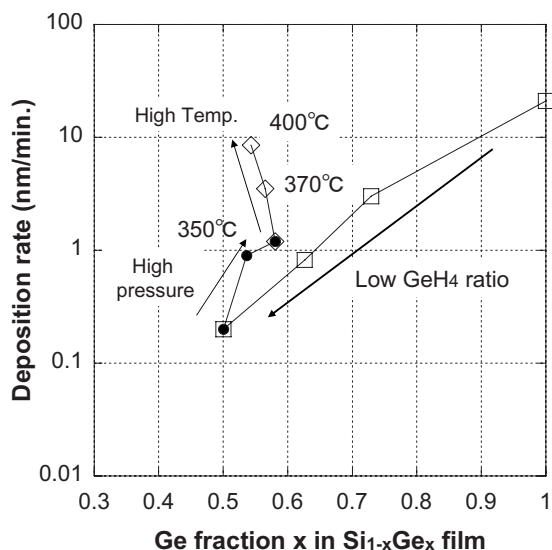
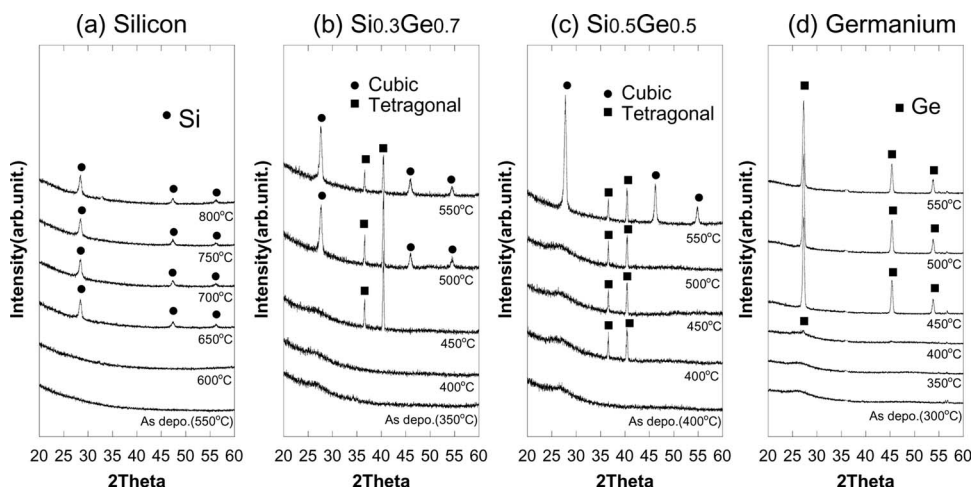


**Figure 6.** Relationship between the deposition rate and Ge fraction in the  $\text{Si}_{1-x}\text{Ge}_x$  films.

sure, and temperature are needed to widely control the composition of  $\text{Si}_{1-x}\text{Ge}_x$  film, especially at temperatures below  $400^\circ\text{C}$ .  $\text{Si}_{0.3}\text{Ge}_{0.7}$  and  $\text{Si}_{0.5}\text{Ge}_{0.5}$  films were eventually obtained at  $350^\circ\text{C}$  and  $400^\circ\text{C}$  with the high deposition rate ( $>1$  nm/min). In the subsequent experiment, we evaluated the solid phase crystallization (SPC) of each  $\alpha$ - $\text{Si}_{1-x}\text{Ge}_x$  film as well as control  $\alpha$ -Si and  $\alpha$ -Ge films.

*SPC of  $\text{Si}_{1-x}\text{Ge}_x$  film.*— Figure 7 shows the XRD patterns of the  $\text{Si}_{1-x}\text{Ge}_x$  films. The films were annealed at various temperatures for 1 h in  $\text{N}_2$ . The phases of the films are summarized in Fig. 8. As shown in Fig. 7a, the  $\alpha$ -Si film started to crystallize at  $650^\circ\text{C}$  with the cubic phase. In contrast, as shown in Fig. 7d,  $\alpha$ -Ge started to crystallize at  $400^\circ\text{C}$ . The lower binding energy of the Ge–Ge bond makes the crystallization temperature low for pure Ge films. In Fig. 7b, the as-deposited  $\text{Si}_{0.5}\text{Ge}_{0.5}$  film was in the amorphous phase and started to crystallize at  $400^\circ\text{C}$  with the tetragonal phase and then changed to the cubic phase at temperatures above  $550^\circ\text{C}$ . In Fig. 7c, as-deposited  $\text{Si}_{0.3}\text{Ge}_{0.7}$  was also in the amorphous phase and started to crystallize at  $450^\circ\text{C}$  with the tetragonal phase and then changed to the cubic phase above  $500^\circ\text{C}$ . These results indicate that the metastable tetragonal phase is easy to crystallize at low temperature, especially in the  $\text{Si}_{0.5}\text{Ge}_{0.5}$  film, while the tetragonal phase is stable at the higher temperature than in the  $\text{Si}_{0.7}\text{Ge}_{0.3}$  film.



## Conclusion

Low-temperature LPCVD of silicon–germanium ( $\text{Si}_{1-x}\text{Ge}_x$ ) and its SPC were investigated using  $\text{SiH}_4$ ,  $\text{SiH}_2\text{Cl}_2$  (DCS), and  $\text{GeH}_4$  gaseous sources.  $\text{SiH}_4$  is a better source gas than DCS for the purpose of film composition tunability. In the  $\text{SiH}_4$ : $\text{GeH}_4$  system, the binary deposition mechanism is well-explained by the enhancement model. The deposition temperature and chamber pressure affect the  $J$  factor, which facilitates independent tuning of the film composition and deposition rate. Amorphous  $\text{Si}_{0.7}\text{Ge}_{0.3}$  and  $\text{Si}_{0.5}\text{Ge}_{0.5}$  films were obtained at  $350^\circ\text{C}$  and  $400^\circ\text{C}$  by adjusting the deposition conditions while keeping the deposition rates high. The amorphous  $\text{Si}_{0.5}\text{Ge}_{0.5}$  film was crystallized by SPC at  $400^\circ\text{C}$  for 1 h in inert ambient. These  $\text{Si}_{1-x}\text{Ge}_x$  films are useful for low thermal budget applications.

**Figure 7.** XRD patterns of films annealed at the different temperature for 1 h. (a) Si, (b)  $\text{Si}_{0.7}\text{Ge}_{0.3}$ , (c)  $\text{Si}_{0.5}\text{Ge}_{0.5}$ , and (d) Ge.

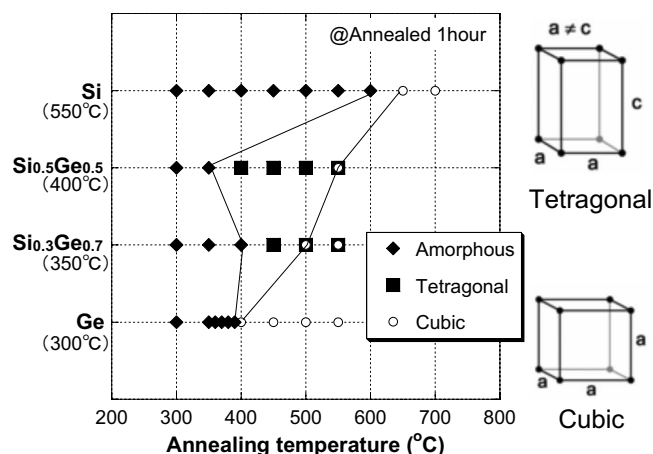


**Figure 8.** Summary of film phases by SPC.

To investigate the stability of the tetragonal phase, the deposition mechanism should be revisited as shown in Fig. 5b. To obtain the  $\text{Si}_{0.5}\text{Ge}_{0.5}$  film, the sum of probabilities for cases (A) and (B) should be the same as that for case (C) and (D). Here, we suppose that the probability of case (D) is still very low and that the deposition of the  $\text{Si}_{1-x}\text{Ge}_x$  film proceeds by cases (B) and (C). In other words, Si and Ge are deposited alternatively, creating a slight periodicity in the film, which relates to the tetragonal phase. Thus, the tetragonal phase is crystallized at the low temperature, especially at the composition of  $x \sim 0.5$ .

### Acknowledgments

The authors acknowledge the contributions made by Dr. Y. Mochizuki and Dr. N. Kasai, NEC Corporation for their research support. A part of this work was supported by the DARPA 3D-ICs program and was done in the Stanford Nanofabrication Facility (SNF) of NNIN.

*NEC Corporation assisted in meeting the publication costs of this article.*

### References

1. T. Mizuno, N. Sugiyama, T. Tezuka, Y. Moriyama, S. Nakaharai, T. Maeda, and S. Takagi, *IEEE Trans. Electron Devices*, **52**, 2690 (2005).
2. J. S. Hamel, Y. T. Tang, and K. Osman, *IEEE Trans. Electron Devices*, **49**, 449 (2002).
3. M. Wolf, R. Brendel, and J. H. Queisser, *J. Appl. Phys.*, **83**, 4213 (1998).
4. T.-J. King, P. McVittie, and K. C. Saraswat, *IEEE Trans. Electron Devices*, **41**, 228 (1994).
5. C. O. Chui and K. C. Saraswat, in *Germanium-Based Technologies: From Materials to Devices*, C. Claeys and E. Simoen, Editors, Elsevier Science, Amsterdam (2007).
6. T. Ghani, M. Armstrong, C. Auth, M. Bost, P. Charvat, G. Glass, T. Hoffmann, K. Johnson, C. Kenyon, J. Klaus, et al., in *Digest of IEEE IEDM 2003*, p. 11.6.1 (2003).
7. T.-J. King, K. C. Saraswat, and J. R. Pfister, *IEEE Electron Device Lett.*, **12**, 584 (1991).
8. Y.-C. Jeon, T.-J. King, and R. T. Howe, *J. Electrochem. Soc.*, **150**, H1 (2003).
9. V. Subramanian and K. C. Saraswat, *IEEE Trans. Electron Devices*, **45**, 1934 (1998).
10. K. Banerjee, S. J. Souri, P. Kapur, and K. C. Saraswat, *Proc. IEEE*, **89**, 602 (2001).
11. M. Tada, H. Yamamoto, T. Takeuchi, N. Furutake, F. Ito, and Y. Hayashi, *J. Electrochem. Soc.*, **154**, D354 (2007).
12. M. Tada, H. Ohtake, F. Ito, M. Narihiro, T. Taiji, Y. Kasama, T. Takeuchi, K. Arai, N. Furutake, N. Oda, et al., *IEEE Trans. Electron Devices*, **54**, 797 (2007).
13. N. M. Russell and W. G. Breiland, *J. Appl. Phys.*, **73**, 3525 (1993).
14. J. Olivares, J. Sangrador, A. Rodriguez, and T. Rodriguez, *J. Electrochem. Soc.*, **148**, C685 (2001).
15. J. Holleman, A. E. T. Kuiper, and J. F. Verweij, *J. Electrochem. Soc.*, **140**, 1717 (1993).
16. S.-M. Jang and R. Reif, *Appl. Phys. Lett.*, **59**, 3162 (1991).
17. M. Cao, A. Wang, and K. C. Saraswat, *J. Electrochem. Soc.*, **142**, 1566 (1995).
18. O. O. Olubuyide, D. T. Danielson, L. C. Kimerling, and J. L. Hoyt, *Thin Solid Films*, **508**, 12 (2006).
19. A. W. Wang, Ph.D. Thesis, Stanford University (1998).
20. *CRC Handbook of Chemistry and Physics*, 72nd ed., D. R. Lide, Editor, CRC Press, Boston (1991).
21. S.-M. Jang, *Appl. Phys. Lett.*, **60**, 707 (1992).